8.2 THE NONLINEAR CHARACTER OF MJO/OCEANIC KELVIN WAVE INTERACTIONS ABOUT THE ENSO CYCLE

Paul E. Roundy* and George N. Kiladis
NOAA/CIRES Aeronomy Laboratory

Introduction

Analysis of data from the TAO (Tropical Atmosphere Ocean) array of moored buoys and other sources suggests that the MJO plays some roll in the development of El Niño, predominantly through the oceanic Kelvin waves that it triggers and through forcing of the ocean surface by the local wind, but there has been little agreement about the details and the extent of its importance. Some of us seem to largely ignore it in favor of lower frequency oceanic processes. Others suggest that it is only important to the timing and initial growth of El Niño (e.g., Bergman et al. 2001), while still others suggest that it is almost entirely responsible for some El Niño events (e.g., Vialard et al. 2001). Unanswered questions to which many of us assume different answers cast doubt on each of these hypotheses.

Strong downwelling oceanic Kelvin waves produced by westerly wind anomalies within the active convective phase of the MJO can couple to the atmosphere in ways that modify their behavior and long-term impacts (e.g., Lau and Shen 1988; Federov and Melville 2000; Roundy and Kiladis 2005). We show that downwelling and upwelling Kelvin waves produce different environmental responses and couple differently to the atmosphere. Differences between their respective coupling processes introduce nonlinearity and may allow a series of the waves under certain circumstances to produce a net positive effect on a trend toward El Niño conditions.

2. Methods

This study includes composite analyses of TAO data, NOAA interpolated OLR, and 1000 hPa winds from the NCEP/NCAR reanalysis.

Beginning with a time series of 20-100 day band TAO dynamic height data at the equator and the dateline (a proxy index for Kelvin waves), we make two different kinds of composites. The first is a simple average. We find all of the dates of local maxima in our Kelvin wave index (most of which correspond to crests of Kelvin waves). We then average wind stress, OLR, and dynamic height over the same dates and lags from those dates.

The second composite applies a regression model that allows for focus on behavior associated with Kelvin waves during specific portions of the ENSO cycle. Assuming the index for Kelvin wave dynamic height at the dateline (k), an ENSO index of Niño 3.4 mean dynamic height (e), and an ENSO trend index ($\dot{e}$, the first time derivative of the ENSO index), the regression model is:

$$y = a_0 + a_1 e + a_2 \dot{e} + a_3 k +$$
$$a_4 k^2 + a_5 k^3 + a_6 k^4 +$$
$$a_7 e \bullet k + a_8 \dot{e} \bullet k + a_9 (e \bullet k)^2 +$$
$$a_{10} (\dot{e} \bullet k)^2 + a_{11} (e \bullet k)^3 + a_{12} (\dot{e} \bullet k)^3 +$$
$$a_{13} (\dot{e} k^2) + a_{14} (\dot{e} k^3) + \varepsilon$$

Each term is physically motivated. Terms 0-3 diagnose the mean and ENSO-related background. Term 3 diagnoses the part of the signals that is linearly related to the Kelvin waves. Terms 4-6 diagnose the higher-frequency signals that are related to the Kelvin wave index, including harmonics and higher-frequency waves. Terms 7 and 8 diagnose modulation of the Kelvin wave-related fields by ENSO and its trend. Further terms diagnose higher-frequency components related to the modulation of the Kelvin waves by interactions with the longer timescale ENSO signal. Linear correlations between the terms are calculated and removed in the order that they are listed, by following the Gram Schmit process. We develop composites by solving for the

*Corresponding Author Address:
Paul E. Roundy, 325 Broadway R/AL3
Boulder, CO 80305-3328

coefficients, then substituting values for the indices consistent with marginally warm and rapidly developing El Niño conditions, and a Kelvin wave crest in dynamic height at the dateline. The background terms are calculated, but not included in the composite plotted here.

3. Summary

The composite average (Figure 1) includes nearly all Kelvin waves in the dataset, regardless of the background states through which they propagate. This result would favor those times when Kelvin waves are most active, but include contributions from all waves. The regression composite (Figure 2) specifically diagnoses the relationships often observed during rapidly developing El Niño conditions.

Figure 1 shows negative and positive OLR anomalies propagating eastward across the Indian Ocean and into the West Pacific basin. Westerly (easterly) wind stress anomalies (from the NCEP/NCAR reanalysis) are nearly collocated with negative (positive) OLR anomalies. Upon arrival of the wind stress anomalies into the West Pacific, oceanic Kelvin waves begin to develop (as suggested by the composite TAO dynamic height anomalies). After the Kelvin waves begin to form, the wind stress and OLR patterns lose their symmetry in time and space. The easterly stress anomalies accelerate across the basin and appear in the Central and East almost immediately after they arrive in the west. The high amplitude positive wind stress anomaly approaching lag 0 and the dateline at nearly constant or decreasing speed is intercepted and stopped by an accelerating trade surge.

In addition to the differences in the easterly and westerly wind stress patterns, the phase speeds of subsequent composite dynamic height anomalies decrease with time. We have found that this is because most high amplitude Kelvin waves are preceded by faster waves and followed by slower ones (Roundy and Kiladis 2005).

Figure 2 shows the regression composite. Specifying rapidly developing El Niño conditions allows this composite to diagnose further asymmetries in the relationships between atmospheric forcing and the Kelvin waves. The negative OLR anomalies of the Indian Ocean active MJO do not last as long as the positive anomalies of the suppressed MJO. This result is consistent with individual events during this stage of ENSO (e.g., 1997 and 2002, Roundy and Kiladis 2005). The suppressed phase of the MJO in the enclosed region labeled (a) moves into the West Pacific, where it induces an easterly wind stress anomaly (as seen in the TAO data) that accelerates quickly across the basin. As the subsequent active phase of the MJO (trajectory b) moves into the West Pacific, a downwelling Kelvin wave forms (seen in regressed dynamic height following trajectory 2). Following the development of the Kelvin wave, the convection and wind stress both decelerate, allowing the wind stress to further amplify the wave by continuing behind its dynamic height crest instead of accelerating eastward. This stress anomaly is not replaced by an easterly stress anomaly along the path of the downwelling wave until it moves east of 150°W.

The phase deceleration of the dynamic height anomalies seen in Figure 1 is even more apparent in Figure 2, suggesting that subsequent waves tend to slow down with time more during periods of strong trend toward El Niño than during other background conditions.

Since Figure 1 contains the patterns averaged over the set of all Kelvin waves in the dataset, and Figure 2 emphasizes periods of strong trend towards El Niño, comparison of the two figures suggests ways that Kelvin waves and their associated forcing disturbances differ with the basic state, and how these waves may impact that state. Both upwelling and downwelling waves may affect their environments. Their combined long-term impacts would depend on the asymmetries noted above, and how these asymmetries change with the ENSO cycle.

Asymmetry in time and longitude is linked to differences in nonlinearity between upwelling and downwelling waves (e.g., Lau and Shen 1988; Federov and Mellville 2000; Roundy and Kiladis 2005). Linear Kelvin waves propagate parallel to isopycnals. When the thermocline shoals sharply to the east, high amplitude downwelling waves can begin to propagate across the isopycnals, forming fronts or zones of eastward advection of temperature (e.g., Federov and Melville 2000). Upwelling waves remain parallel to the isopycnals in such conditions, and mainly affect temperature through raising the thermocline. Eastward advection of temperature in downwelling waves allows them to systematically impact SST. Through their influence on SST, they modulate atmospheric convection and thus the nature of the wind stress forcing (like the advective mode of Lau and Shen 1988). This slows the forcing down, extending its duration in the vicinity of the Kelvin wave, thus allowing for further wave amplification. This coupling process requires a sufficiently strong zonal SST gradient prior to the development of the Kelvin wave.

The easterly phase of the MJO is responsible for generation of upwelling intraseasonal Kelvin waves, but it does not couple in the same way to the waves as the westerly phase couples do downwelling waves, so it actually accelerates across the basin. This asymmetry can enhance the impact of downwelling waves and allows a series of the waves to produce a net positive impact on a trend toward El Niño. Trade surges related to the suppressed phase of the MJO and other disturbances would disrupt the coupling of the downwelling Kelvin waves to atmospheric forcing, so the timing of these surges relative to the development of downwelling waves would greatly impact the ability of these waves to amplify enough to warm the waters of the eastern basin.

Figure 1 suggests that the coupling of most downwelling Kelvin waves to the atmosphere is disrupted before the waves reach the dateline. In contrast, Figure 2 suggests that waves that occur during periods of strongest trend toward El Niño conditions remain coupled to the wind stress forcing even into the eastern basin. Since subsequent Kelvin waves tend to decelerate with time, the increased basin transit time would enhance the likelihood of their being influenced by a trade surge, limiting the strength and longevity of a trend toward El Niño.

Kelvin waves occur during most years, including those years when El Niño conditions do not develop. We propose that their impacts on a trend toward El Niño conditions depend largely on the strength and duration of their coupling to westerly wind anomalies, as modulated by atmospheric convection.

Acknowlegements

Funding for this work was provided by the NOAA office of Global Programs under grant GC01-351 to GNK. The TAO Project Office of NOAA/PMEL provided the mooring time series data.

Works Cited

Bergman, J.W., H.H. Hendon, and K.M. Weickman, 2001: Intraseasonal air-sea interactions at the onset of El Niño. *J. Climate*, **14**, 1702-1718. *Climate Dynamics*. **15**, 205-225.

Federov, A.V., and W.K. Melville, 2000: Kelvin fronts on the equatorial thermocline. *J. Phys. Oceanog.*, **30**, 1692-1705.

Lau, K.-M., and S. Shen, 1988: On the dynamics of intraseasonal oscillations and ENSO. *J. Atmos. Sci.*, **45**, 1781-1797.

Roundy, P.E., and G.N. Kiladis, 2005: Observed relationships between oceanic Kelvin waves and atmospheric forcing. Submitted to *J. Climate* May 2005.

Vialard, J., C. Menkes, J.-P. Boulanger, P. Delecluse, E. Guilyardi, M. J. McPhaden, and G. Madec, 2001: A model study of oceanic mechanisms affecting equatorial Pacific sea surface temperature during the 1997-1998 El Niño. *J. Phys. Oceanog.*, **31**, 1649-1672.

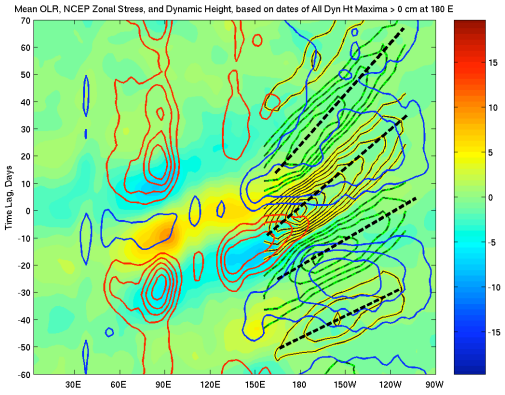

Figure 1 Composite average OLR (shading, Wm^{-2}, negative values in blue), wind stress (m^2s^2, westerly contoured in red, easterly in blue), and dynamic height (cm, positive anomalies contoured in black, with a yellow highlight, and negative anomalies contoured with a dash-dotted line and a green highlight. Wind stress contours are included every 1 m^2s^{-2}, with the zero line omitted. Dynamic height contours are plotted every quarter cm, with the zero line omitted. Data on all dates of 20-100 day band dynamic height maxima at the dateline were included. The solid line represents the trajectory of a negative OLR and wind stress anomaly, and the heavy dashed lines represent trajectories of dynamic height anomalies.

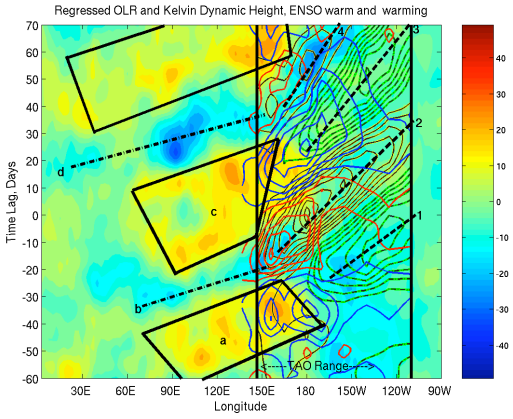

Figure 2 Longitude-time lag regression composite of OLR, the zonal component of the wind stress, and dynamic height. The wind stress contour interval is 3 m^2s^{-2}, with minimum contours at +/- 1.5 m^2s^{-2}. Dynamic height contours are drawn every 1 cm, with the zero line omitted. This composite is based on an index of Kelvin wave dynamic height at the equator and the dateline, and includes terms with subscripts 3-14 for regressed OLR and 3-8 and 13-14 for the other variables. Dash-dotted lines and irregular boxes (some labeled a-d) track active and suppressed phases of the MJO (respectively), while dashed trajectory lines (labeled 1-4) track Kelvin wave dynamic height anomalies.